Progress In Electromagnetics Research M, Vol. 107, 167–179, 2022

Load-Independence-Based Composite Compensation Network and Control Strategy for Wireless Electric Vehicle Charging System

Wenzhou Lu*, Runmin Liu, Xiangxiu Chen, Jian Zhao, Qigao Fan, and Chendawei Zhang

Abstract—Nowadays, wireless charging for electric vehicles has become popular in numerous situations by reason of safety and convenience. In this article, a composite compensation network and the corresponding charging control strategy aiming at optimizing the transmitting efficiency of the system and achieving constant current (CC) output and constant voltage (CV) output are proposed. First, the composite compensation network is analyzed by the equivalent circuit model as a reference. Second, based on the realization of CC/CV output, by analyzing the relationship between charging current/voltage and duty cycles of both DC-DC converters, the optimal duty cycles of both converters can be found. The purpose is to obtain the maximum transmission efficiency. Finally, the experimental results show good agreement with theoretical analysis, proving that the proposal can realize CC/CV charging and optimize the transmission efficiency.

1. INTRODUCTION

In recent years, electric vehicles (EVs) wireless charging technology has become a new research hotspot, especially in directions of magnetic coupling structure [1–4], compensation network [5–8], and transmitting efficiency optimization [9–11]. In the research of magnetic coupling structure, the application of double D (DD) coil to EVs wireless charging system is proposed for the first time [1]. A DD coil has better anti-offset characteristics and a larger ampler charging area than a circle coil, which can make full use of the chassis area of EVs. An optimization method based on the finite element analysis is proposed, aiming to optimize the volume of circle and bar magnetizers, which maintains a uniform distribution of magnetic flux density in magnetizer and minimizes the loss of the magnetizer [2]. The TP (Tripolar) coil is optimized in the aspect of coil offset resistance [3]. A patterned soft magnetic metal is designed to block the path of induced current to reduce eddy current losses. The optimized soft magnetic metal is 84% thinner than the ferrite of the same size, and the transmission efficiency is similar to that of the ferrite material [4]. In the research of compensation network, the inductor-capacitance-capacitance (LCC) compensation network is proposed to eliminate the mutual inductance between the compensation coil and the transmitting or receiving coils by decoupling [5–8]. Another advantage is that it can provide a compact structure of the system when the compensation coils and transmitting (Tx) coil/receiving (Rx) coil are overlapped. In the research of transmitting efficiency optimization, a cascaded Boost-Buck DC-DC converter for impedance matching is proposed in [9]. The working principle of the signal-phase full-bridge rectifier is analyzed [10, 11], which replaces the traditional uncontrollable rectifier with a controllable rectifier. Without an additional DC-DC converter, the secondary side achieves impedance matching more accurately by changing the output voltage of the controllable rectifier and the phase between the output voltage and output current.

Received 20 November 2021, Accepted 10 January 2022, Scheduled 21 January 2022
* Corresponding author: Wenzhou Lu (luwenzhou@126.com).
The authors are with the Key Laboratory of Advance Process Control for Light Industry (Ministry of Education), School of Internet of Things Engineering, Jiangnan University, Wuxi 214122, China.

In order to satisfy the CC/CV charging requirement [12–14] of the lithium battery of EVs wireless charging system, the inductor-capacitance-inductor (LCL)-LCL and LCL-S compensation network are used to realize CC and CV charging, respectively [15]. They are combined using high-frequency AC switches. However, the secondary side requires more components using the method, which will increase the cost of EVs. A T-type compensation network based on series-series (S-S) compensation network is proposed in [16]. By cascading multiple T-type networks on the secondary side, a compensation network with CC/CV output characteristics can be obtained, and then the compensation network can be switched by high-frequency AC switches to achieve CC/CV charging. But the obvious disadvantage is that the secondary side is too complicated to install in the limited space of EVs. Therefore, a passive component optimization method for S-LCC compensation network is proposed to reduce the cost of the entire system [17], which also achieves CC/CV charging. Primary side load estimation method is used to control the full-bridge converter and achieve CC/CV charging of S-S and series-parallel (S-P) compensation networks, respectively [18]. Moreover, the method collects the output voltage and output current values of the full-bridge converter, which requires a high accuracy with hardware and system parameters. A load estimation and coils decoupling method is proposed to achieve the independent control of primary and secondary, realizing CC/CV charging. However, sampling six corresponding parameters in the entire charging process is needed, which makes the method complex. Zhao et al. [19] adopt switching the three coils structure and S-S compensation network that can realize selecting CC/CV charging mode by comparing estimated equivalent load value with the set load value. Furthermore, the full-bridge controllable rectifier is controlled based on double-sided LCC compensation network to realize CC/CV charging and optimize the transmission efficiency simultaneously [20]. However, the method is only suitable for the systems allowing the voltage and current to fluctuate within a certain range. Huang et al. [21] propose that variable capacitors are connected in series at the secondary side, and impedance matching is carried out through the semi-active controllable rectifier at the secondary side, which maximizes the constant power output and power transmission efficiency of the system. Closed-loop control is carried out on the DC-DC converter of the primary side by using the wireless communication mode of the primary side and secondary side. Proportional-Integral (PI) control is carried out on the DC-DC converter of the secondary side which can achieve CC/CV charging. This control method also needs to be realized by wireless communication [22]. A method is proposed to control the full-bridge inverter with variable step size perturbation observation method [23] for the primary side and to control the semi-active controllable rectifier with PI for the secondary side. Besides, CC charging can be realized by controlling the secondary side.

Considering the issues of the current research, the purpose of this article is to propose a load-independence-based composite compensation network and the control strategy to simplify the charging control method, reduce the passive components on the secondary side, and obtain higher transmission efficiency of the wireless charging system. The composite compensation network is composed of S-S and LCL-S compensation networks, which have load independence characteristics. Without additional passive components, these two networks can be combined using high-frequency AC switches. In this article, the output characteristics of these two networks are derived and analyzed theoretically, and the corresponding control methods are proposed. Besides, the theory is verified by simulation. Finally, an experimental platform is built, the load-independence of the proposed composite compensation network and the feasibility of charging control strategy are verified.

2. DESIGN OF COMPENSATION NETWORK FOR WIRELESS CHARGING SYSTEM

Generally, there are two working states during the charging process. One is charged by the constant current (CC mode): the voltage of battery increases in process of charging. The other is charged by the constant voltage (CV mode): when the voltage of battery increases to a certain value, the battery starts to be charged with constant voltage, and the charging current decreases in the process of charging. The equivalent load of battery increases during the whole charging profile. In order to satisfy the CC/CV requirement, S-S and LCL-S compensation networks are used to charge lithium batteries. The proposed compensation network includes the following three merits:

1) The passive components of the composite compensation network are mainly concentrated on

the primary side while the secondary side has no new passive components. In the case of EVs, the secondary side is installed on the chassis of EV, which contributes to reducing the costs of the system.

2) In respect of the charging control, the proposed composite compensation network is beneficial to reducing the complexity of control strategy, and thus the control strategy is relatively uncomplicated, which can enhance the stability of system.

3) The control strategy based on S-S and LCL-S compensation networks is applicable to other composite compensation networks.

2.1. S-S Compensation Network

S-S compensation network is shown in Fig. 1, where u_s is the input source of the primary side; u_e is the output voltage of the secondary side; C_1 and C_2 are the resonant capacitances; L_1 and L_2 are the self-inductances of Tx and Rx coils, respectively; R_1 and R_2 are the high frequency equivalent resistances of Tx and Rx coils, respectively; M is the mutual inductance of transfer coils; Z_t is the equivalent impedance from secondary side to primary side; R_e is the output equivalent impedance of secondary side; i_1 and i_2 are the currents of primary and secondary sides, respectively.

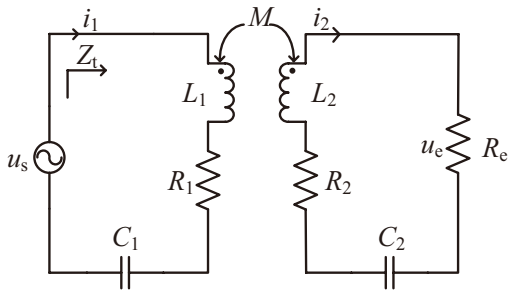

Figure 1. S-S compensation network.

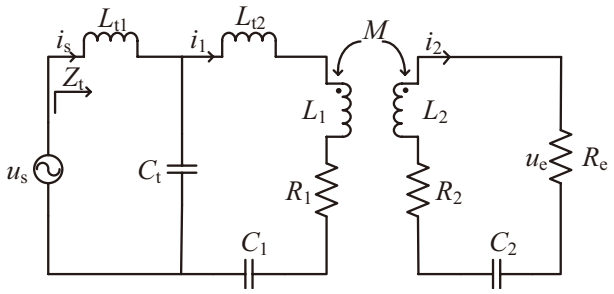

Figure 2. LCL-S compensation network.

Using Kirchhoff Voltage Law (KVL), the equivalent circuit shown in Fig. 1 can be expressed as

$$\begin{cases} u_s = \left(\dfrac{1}{j\omega C_1} + j\omega L_1 + R_1\right) i_1 - j\omega M i_2 \\ j\omega M i_1 = \left(\dfrac{1}{j\omega C_2} + j\omega L_2 + R_2 + R_e\right) i_2 \end{cases} \tag{1}$$

where ω is the system angular frequency, $\omega = 2\pi f$, and f is the resonance frequency. Assume that parameters of the components satisfy the resonance condition: $j\omega L_1 + 1/j\omega C_1 = 0$, $j\omega L_2 + 1/j\omega C_1 = 0$, and the following gain expressions can be obtained.

$$\begin{cases} G_{11} = \dfrac{u_e}{u_s} = \dfrac{i_2 R_e}{u_s} = \dfrac{j\omega M R_e}{R_1(R_e + R_2) + (\omega M)^2} \\ G_{12} = \dfrac{i_2}{u_s} = \dfrac{j\omega M}{R_1(R_e + R_2) + (\omega M)^2} \\ G_{21} = \dfrac{u_e}{i_1} = \dfrac{i_2 R_e}{i_1} = \dfrac{j\omega M R_e}{R_2 + R_e} \\ G_{22} = \dfrac{i_2}{i_1} = \dfrac{j\omega M}{R_2 + R_e} \end{cases} \tag{2}$$

According to the gain G_{12}, when the high frequency equivalent resistances of transmitting and receiving coils can be ignored, i_2 is only related to u_s, M, and ω. Thus, $G_{12} = i_2/u_2 \approx j/\omega M$. If the system is built, the parameters u_s, M, and ω will not change, which derives that i_2 has the load-independence characteristic. Besides, according to the gains G_{11} and G_{21}, the equivalent impedance from secondary side to primary side Z_t is calculated as follows:

$$Z_t = \frac{G_{21}}{G_{11}} = \frac{R_1(R_2 + R_e) + (\omega M)^2}{R_2 + R_e} \tag{3}$$

Equation (3) implies that Z_t is resistive, which means that the zero phase difference between input voltage and current of primary side can be achieved.

2.2. LCL-S Compensation Network

Adding compensation inductance L_{t1} and L_{t2} and compensation capacitance C_t to S-S compensation network, LCL-S compensation network can be obtained as shown in Fig. 2. Let $Z_1 = j\omega L_{t2} + j\omega L_1 + 1/j\omega C_1 + R_1$, $Z_2 = j\omega L_2 + 1/j\omega C_2 + R_2$, using KVL, and the equivalent circuit mode shown in Fig. 2 can be expressed as

$$\begin{cases} u_s = j\omega L_{t1} i_s + \dfrac{1}{j\omega C_t}(i_s - i_1) \\ \dfrac{1}{j\omega C_t}(i_s - i_1) + j\omega M i_2 = Z_1 i_1 \\ j\omega M i_1 = (R_e + Z_2) i_2 \end{cases} \tag{4}$$

Let $L_{t1} = L_{t2} = L_t$, when the system is working at the resonance frequency, $j\omega L_{t1} = j\omega L_{t2} = -1/j\omega C_t$, $j\omega L_1 + 1/j\omega C_1 = 0$, $j\omega L_2 + 1/j\omega C_1 = 0$, it is easy to obtain the gain expressions as follows:

$$\begin{cases} G_{11} = \dfrac{u_e}{u_s} = \dfrac{i_2 R_e}{u_s} = \dfrac{M R_e}{(R_e + R_2) L_t} \\ G_{12} = \dfrac{i_2}{u_s} = \dfrac{M}{(R_e + R_2) L_t} \\ G_{21} = \dfrac{u_e}{i_s} = \dfrac{i_2 R_e}{i_s} = \dfrac{(\omega M)(\omega L_t) R_e}{R_1(R_e + R_2) + (\omega M)^2} \\ G_{22} = \dfrac{i_2}{i_s} = \dfrac{(\omega M)(\omega L_t)}{R_1(R_e + R_2) + (\omega M)^2} \end{cases} \tag{5}$$

From the gain G_{11}, if the high frequency equivalent resistances of Tx and Rx coils can be ignored, u_e can be only related to u_s, M, L_{t1}, and L_{t2}. If the system is built, the parameters u_s, M, and ω will be constant, which achieve that u_e has the load-independence characteristic. In addition, as calculated in G_{11} and G_{21}, the equivalent impedance from secondary side to primary side Z_t can be expressed as

$$Z_t = \frac{G_{21}}{G_{11}} = \frac{(\omega L_t)^2 (R_2 + R_e)}{R_1(R_2 + R_e) + (\omega M)^2} \tag{6}$$

According to Eq. (6), Z_t is resistive, which derives that zero phase difference between input voltage and current of primary side can be achieved.

The analysis above shows that S-S and LCL-S compensation networks have the load-independence characteristics, which can satisfy the charging requirements of lithium batteries. Therefore, the aforementioned two compensation networks are combined in one system by means of switching. As shown in Fig. 3, the composite compensation network wireless charging system is obtained, where U_{in}

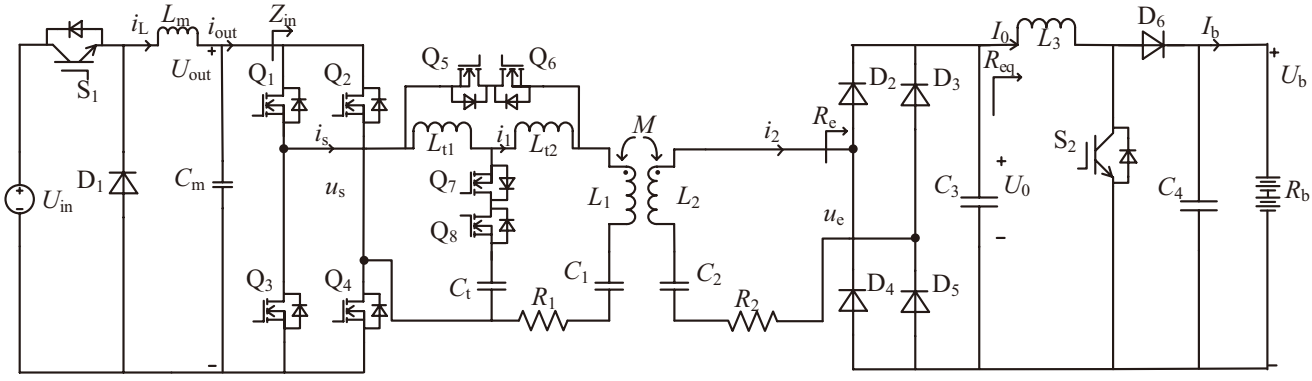

Figure 3. Composite compensation network wireless charging system.

is the DC input source; L_m is the inductance of Buck rectifier; C_m is the capacitor of Buck converter; i_L is the current passing through L_m; i_{out} is the output current of Buck converter; U_{out} is the output voltage of Buck converter; C_3 and C_4 are stabilized capacitors; R_{eq} is the input equivalent resistance of Boost converter; I_0 is the input current of Boost converter; U_0 is the input voltage of Boost converter; R_b is the equivalent resistance of the battery; I_b is the charging current; U_b is the charging voltage.

When MOSFET Q_5 and Q_6 turn on, and Q_7 and Q_8 turn off, the system will operate in CC mode. Inversely, when MOSFET Q_5 and Q_6 turn off, and Q_7 and Q_8 turn on, the system will operate in CV mode.

3. ANALYSIS OF WIRELESS CHARGING CONTROL SYSTEM

Under the premise of achieving the requirement of CC/CV output, the article analyzes and optimizes the transmitting efficiency further, which can make the system more reliable and stable. According to Eq. (2), the transmitting efficiency $\eta_{\text{S-S}}$ of S-S compensation network can be derived as

$$\eta_{\text{S-S}} = \frac{P_{out}}{P_{in}} = G_{11} \cdot G_{22} = \frac{(\omega M)^2 R_e}{R_1(R_2 + R_e)^2 + (\omega M)^2(R_2 + R_e)} \tag{7}$$

Similarly, from Eq. (5), it is easy to obtain the transmitting efficiency $\eta_{\text{LCL-S}}$ of S-S compensation network as follows:

$$\eta_{\text{LCL-S}} = \frac{P_{out}}{P_{in}} = G_{11} \cdot G_{22} = \frac{(\omega M)^2 R_e}{R_1(R_2 + R_e)^2 + (\omega M)^2(R_2 + R_e)} \tag{8}$$

Equations (7) and (8) prove that the expressions of $\eta_{\text{S-S}}$ and $\eta_{\text{LCL-S}}$ are the same, and the only variable in the expressions is R_e (changes in the equivalent resistance of battery will change R_e). For the purpose of showing the relationship between η ($\eta = \eta_{\text{S-S}} = \eta_{\text{LCL-S}}$), M, and R_e visually, Fig. 4 is drawn according to Eq. (8).

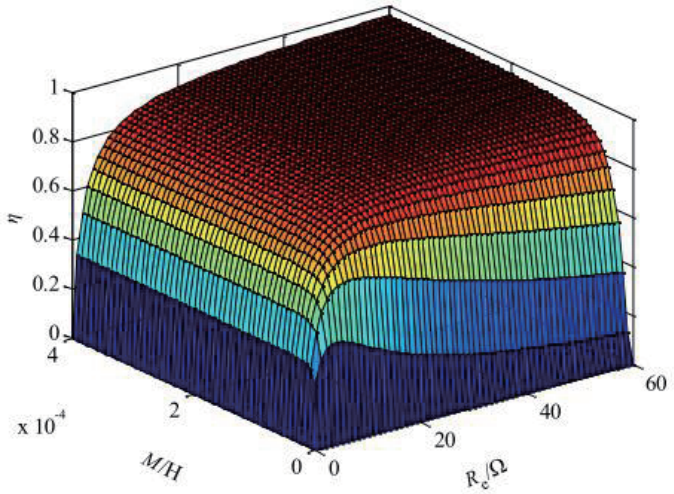

Figure 4. The relationship between η, M and R_e.

It can be seen from Fig. 4 that when M is constant, there is an optimal R_e to make η reach the maximum value of the corresponding curve.

3.1. Optimization of Transmission Efficiency by Matching Load Impedance

The above analysis reveals that two expressions of $\eta_{\text{S-S}}$ and $\eta_{\text{LCL-S}}$ are the same. Thus, let $d\eta/dR_e = 0$, and an expression can be obtained.

$$R_{e\text{-}opt} = \sqrt{R_2^2 + \frac{R_2(\omega M)^2}{R_1}} \tag{9}$$

$R_{e\text{-}opt}$ is the optimal impedance for the maximum transmitting efficiency.

Assuming that the diode rectifier loss of secondary side is ignored, the input current and voltage expressions of Boost converter can be expressed as

$$I_0 = \frac{1}{\pi}\int_0^{\pi}\sqrt{2}I_2\sin(\omega t)d(\omega t) = \frac{2\sqrt{2}I_2}{\pi} \tag{10}$$

$$U_0 = \frac{\pi}{2\sqrt{2}}U_e \tag{11}$$

where I_2 is the root mean square of i_2; U_e is the root mean square of u_e. Additionally, an equation can be derived as

$$I_0^2 R_{eq} = I_2^2 R_e \tag{12}$$

Substituting Eq. (10) into Eq. (12) and simplifying, R_e can be rewritten as

$$R_e = \frac{8}{\pi^2}R_{eq} \tag{13}$$

Considering the characteristic of Boost converter, the following equations are obtained.

$$I_0 = \frac{U_b}{U_0}I_b = \frac{1}{1-\alpha}I_b \tag{14}$$

$$U_0 = (1-\alpha)U_b \tag{15}$$

$$R_e = \frac{8}{\pi^2}R_{eq} = \frac{8}{\pi^2}R_b(1-\alpha)^2 \tag{16}$$

Substituting Eq. (16) into Eq. (8) and simplifying, η can be rewritten as:

$$\eta = \frac{8}{\pi^2}\cdot\frac{(\omega M)^2 R_b(1-\alpha)^2}{R_1\left[R_2+\frac{8R_b}{\pi^2}\cdot(1-\alpha)^2\right]^2+(\omega M)^2\left[R_2+\frac{8R_b}{\pi^2}\cdot(1-\alpha)^2\right]} \tag{17}$$

Equation (17) implies that the maximum transmission efficiency cannot be achieved by adjusting α when R_b is smaller or larger than the critical value, then the system is unreliable when R_b is sufficiently large or small.

3.2. Control Strategy

Combined with Eqs. (14) and (15), when α changes, the charging current and voltage will also change. In order to maintain CC/CV charging and optimize transmission efficiency of the system simultaneously, it is necessary to adjust the duty cycle D of Buck converter to make the load current and voltage adjustable. Thus, the relationship between D, I_b, and U_b should be analyzed further.

U_s is the root mean square of u_s, which can be described as

$$U_s = \frac{2\sqrt{2}}{\pi}U_{in}D \tag{18}$$

Substituting Eqs. (10), (14), (16), and (18) into Eq. (2) and simplifying, the following equation about I_b, R_b, D, and α is obtained.

$$I_b = \frac{8}{\pi^2}\cdot\frac{\omega M U_{in}D(1-\alpha)}{\left[(\omega M)^2+R_1\left(R_2+\frac{8}{\pi^2}R_b(1-\alpha)^2\right)\right]} \tag{19}$$

As can be seen from Eq. (19) that when R_b is constant, I_b can reach the reference value $I_{b\text{-}ref}$ by adjusting D and α.

Substituting Eqs. (11), (15), (16), and (18) into Eq. (5), the equation about U_b, R_b, D, and α can be derived as follows:

$$U_b = \frac{8}{\pi^2}\cdot\frac{MU_{in}DR_b(1-\alpha)}{L_t\left[R_2+\frac{8}{\pi^2}R_b(1-\alpha)^2\right]} \tag{20}$$

From Eq. (20), it is obvious that when R_b is constant, U_b can reach the reference value $U_{b\text{-}ref}$ by adjusting D and α.

The analysis of Eqs. (19) and (20) implies that CC/CV charging can be achieved by adjusting the duty cycles of Buck and Boost converters.

From the analysis before, it can be concluded that transmission efficiency optimization can be achieved by adjusting the duty cycle of Boost converter. Therefore, for the purpose of optimizing the transmission efficiency further based on CC/CV charging modes, it is essential to calculate the optimal duty cycles D_{opt} and α_{opt} corresponding to each R_b during the charging profile. Substituting Eq. (9) into Eq. (16), the equation of α_{opt} is expressed.

$$\alpha_{opt} = 1 - \left(\frac{\pi^2}{8R_b}\right)^{\frac{1}{2}} \cdot \left[R_2^2 + \frac{R_2(\omega M)^2}{R_1}\right]^{\frac{1}{4}} \tag{21}$$

R_b is the only variable in Eq. (21). If R_b changes, α_{opt} should change accordingly to the optimized transmitting efficiency.

Substituting Eqs. (16) and (21) into Eqs. (19) and (20), the equations of $D_{opt\text{-CC}}$ and $D_{opt\text{-CV}}$ based on CC/CV charging modes can be calculated respectively.

$$\begin{aligned} D_{opt\text{-CC}} &= \frac{\pi^2}{8} \cdot \frac{\left[(\omega M)^2 + R_1(R_2 + R_{e\text{-}opt})\right] I_{b\text{-}ref}}{\omega M U_{in}(1-\alpha_{opt})} \\ &= \frac{\pi}{\sqrt{8}} \cdot \frac{\left[(\omega M)^2 + R_1\left(R_2 + \left(R_2^2 + \dfrac{R_2(\omega M)^2}{R_1}\right)^{\frac{1}{2}}\right)\right] I_{b\text{-}ref}}{\left(\dfrac{1}{R_b}\right)^{\frac{1}{2}} \omega M U_{in}\left[R_2^2 + \dfrac{R_2(\omega M)^2}{R_1}\right]^{\frac{1}{4}}} \end{aligned} \tag{22}$$

$$\begin{aligned} D_{opt\text{-CV}} &= \frac{(R_{e\text{-}opt} + R_2)(1-\alpha_{opt}) L_t U_{b\text{-}-ref}}{R_{e\text{-}opt} M U_{in}} \\ &= \frac{\pi}{2\sqrt{2}} \cdot \frac{\left(\dfrac{1}{R_b}\right)^{\frac{1}{2}}\left[R_2 + \left(R_2^2 + \dfrac{R_2(\omega M)^2}{R_1}\right)^{\frac{1}{2}}\right] L_t U_{b\text{-}ref}}{M U_{in}\left(R_2^2 + \dfrac{R_2(\omega M)^2}{R_1}\right)^{\frac{1}{4}}} \end{aligned} \tag{23}$$

Therefore, the composite compensation network wireless charging control system shown in Fig. 5 is proposed in this article. The system is composed by DC input source U_{in}, a Buck converter, a full-bridge inverter, Tx and Rx coils, a rectifier, a Boost converter, and battery. The primary side control involves outputting Buck converter duty cycle signal, outputting Pulse Width Modulation (PWM) complementary signals to full-bridge inverter, and outputting switch control signals of K_1 and K_2. The secondary side control includes outputting Boost converter duty cycle signal. CC/CV charging and transmission efficiency optimization control block diagrams are shown in Fig. 6.

4. SIMULATION AND EXPERIMENT

CC/CV charging modes are separated for simulation to verify the correctness of the theory because it is beneficial to making the simulation results more intuitive. Parameters of simulation and experiment are shown in Table 1.

4.1. Simulation Results

1) The CC charging mode: Based on the parameters given in Table 1, the CC charging waveform is plotted in Fig. 7. First, I_b is constant when the load increases from 35 Ω to 50 Ω. Second, Fig. 7 shows the current charging waveform under the ideal condition (R_1 and R_2 are ignored), and the I_b value is closer to the reference value (2 A) than non-ideal condition.

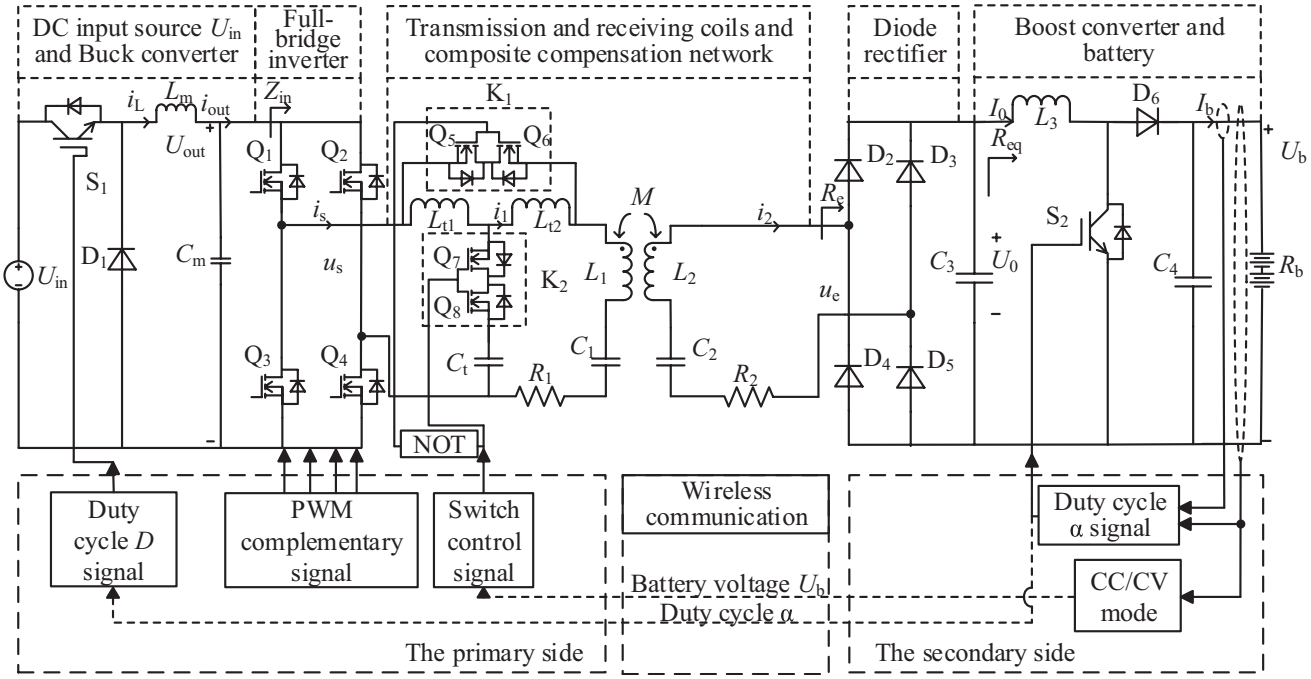

Figure 5. Composite compensation network wireless charging control system.

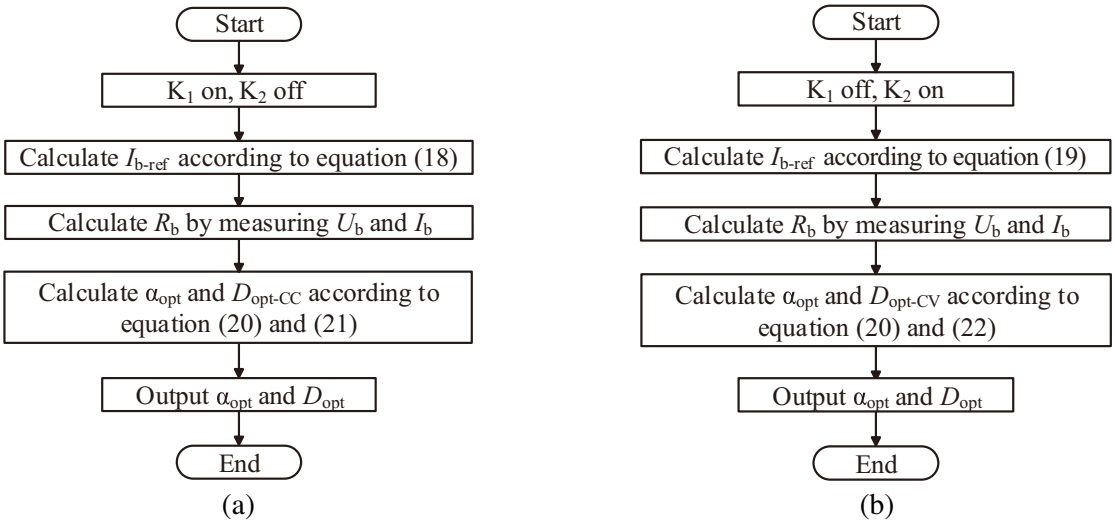

Figure 6. CC/CV charging and transmission efficiency optimization control block diagrams. (a) CC charging control block diagram. (b) CV charging control block diagram.

2) The CV charging mode: When the load increases from 225 Ω to 300 Ω, as shown in Fig. 8, U_b can keep at a constant value. Moreover, it can be shown that the voltage charging waveform under the ideal condition (R_1 and R_2 are ignored), and the U_b value is closer to the reference value (100 V) than non-ideal condition.

The waveforms of the CC charging and the CV charging after optimization are plotted in Fig. 9 and Fig. 10, respectively. The results reveal that I_b and U_b can be maintained at 2 A and 100 V respectively when the proposed strategy is adopted.

Figure 11(a) depicts the trend of the transmission efficiency before and after CC charging optimization. Similar to Fig. 11(a), the transmission efficiency before and after CV charging

Table 1. Parameters of simulation and experiment.

Parameters	Simulation (S-S/LCL-S)	Experiment (S-S/LCL-S)
U_{in}	200 V	110 V
f	86.2 kHz	86.2 kHz
M/h	55×10^{-6} H	130 cm
L_1	176×10^{-6} H	181×10^{-6} H
L_2	176×10^{-6} H	182×10^{-6} H
L_{t1}	none/0.1×10^{-3} H	none/0.1×10^{-3} H
L_{t2}	none/0.1×10^{-3} H	none/0.1×10^{-3} H
R_1	2.3 Ω	2.3 Ω
R_2	1 Ω	1 Ω

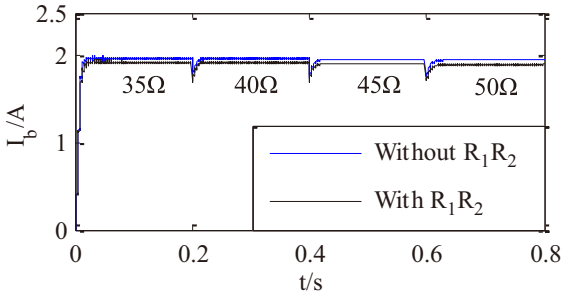

Figure 7. The CC charging waveform.

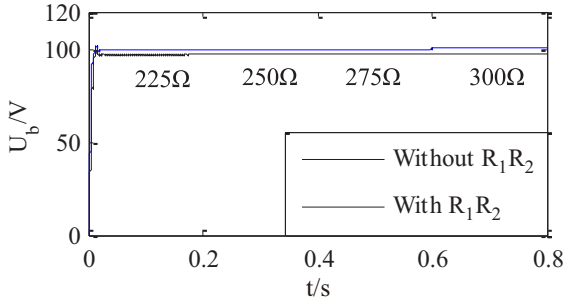

Figure 8. The CV charging waveform.

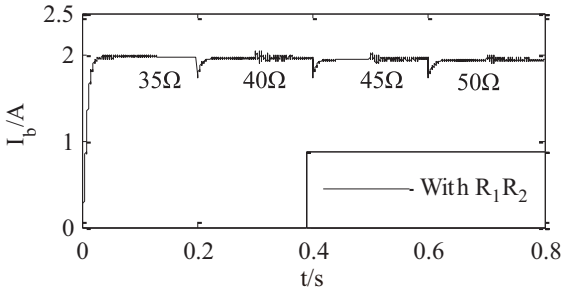

Figure 9. The optimal CC charging waveform.

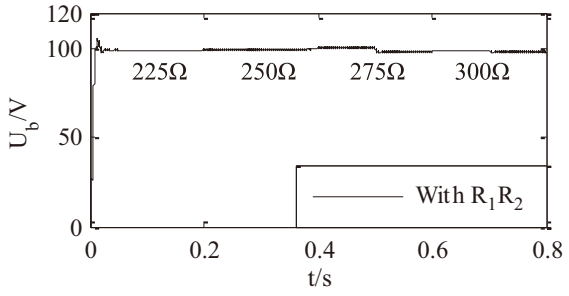

Figure 10. The optimal CV charging waveform.

optimization is plotted, as shown in Fig. 11(b). Both Fig. 11(a) and Fig. 11(b) imply that the transmission efficiency is obviously improved by using the proposed control strategy.

The following conclusions can be drawn through the simulation:

1) In CC charging mode, the high-frequency equivalent resistances (R_1 and R_2) will have an influence on the magnitude of the charging current value, which can also be reflected in Eq. (19). However, when R_1 and R_2 are considered, the values of R_1 and R_2 are very small, which can be ignored. Thus, the difference between the charging current value and reference value is negligible. Therefore, S-S compensation network has the load-independence characteristic. Similar to CC charging mode, CV charging mode has no difference in these rules.

2) In CC charging mode, I_b is constant when the load increases from 35 Ω to 50 Ω, as shown in Fig. 7 and Fig. 9. Similarly, in CV charging mode, U_b is constant when the load increases from 225 Ω

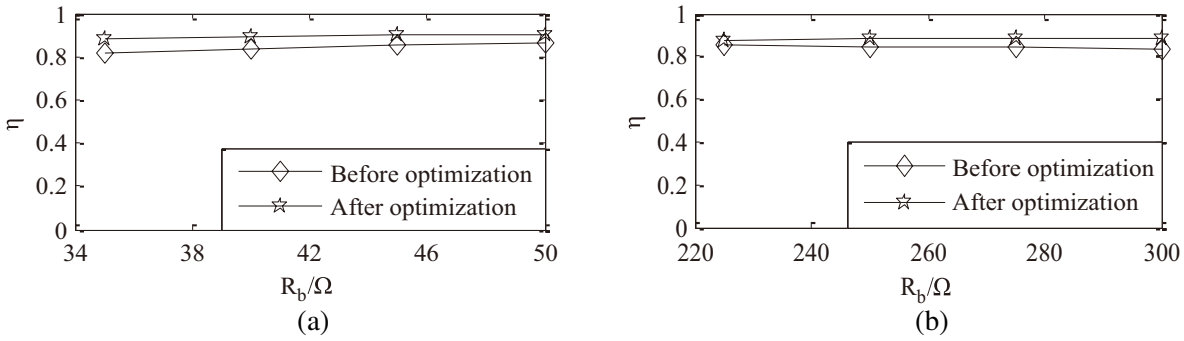

Figure 11. The comparison waveform of transmission efficiency before and after optimization. (a) CC charging optimization. (b) CV charging optimization.

to 300 Ω, as shown in Fig. 8 and Fig. 10. It can be obviously found that CC/CV charging is maintained with arbitrary load impedance in the dynamic range.

3) In terms of transmission efficiency, the transmission efficiencies of CC/CV charging mode can exceed 82% before optimization, as shown in Fig. 11(a) and Fig. 11(b). It can imply that CC/CV charging is maintained with the compensation network, and this compensation network is effective. In addition, the transmission efficiencies of CC/CV charging modes exceed 88%, which have an evident improvement compared with the transmitting efficiency before optimization.

4.2. Experiment Results

The experimental platform of composite compensation network wireless charging control system is built, as shown in Fig. 12. Detailed parameters of the compensation topology are given in Table 1. TMS320F28335 is adopted as the controller for data acquisition and comparison. The experimental platform obtains the DC input source from the three-phase power through three-phase full-bridge, and the power is adjusted by Buck converter. The DC power is transferred to AC power through the full bridge inverter, and the AC power is transmitted from the Tx coil to the Rx coil through the magnetic coupling. Then, the AC power is rectified into DC power through the diode rectifier, and the DC power is sent to the Boost converter. According to the optimized efficiency, the equivalent load is adjusted by the Boost converter.

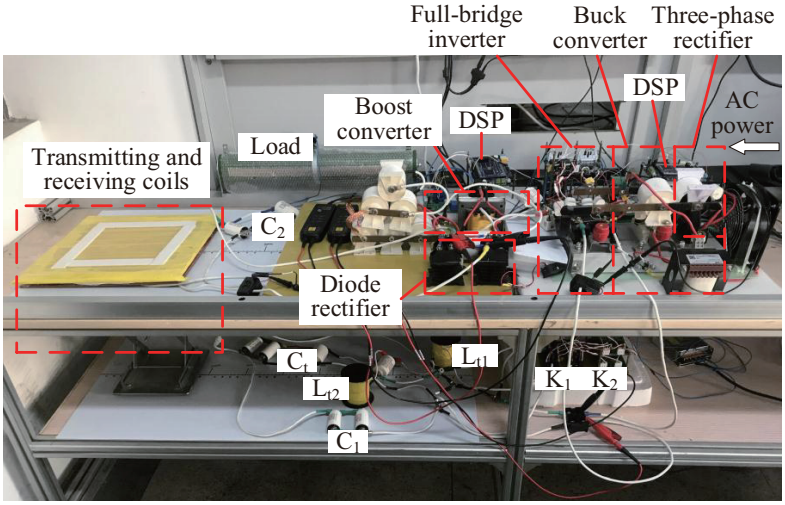

Figure 12. The experimental platform of composite compensation network wireless charging control system.

The voltage/current waveforms of S-S/LCL-S compensation network are shown in Fig. 13 and Fig. 14. It can be seen from Fig. 13 and Fig. 14 that u_s and i_s are in phase, and additionally the phase between u_2 and i_2 is the same. Therefore, the system operates in the resonance state.

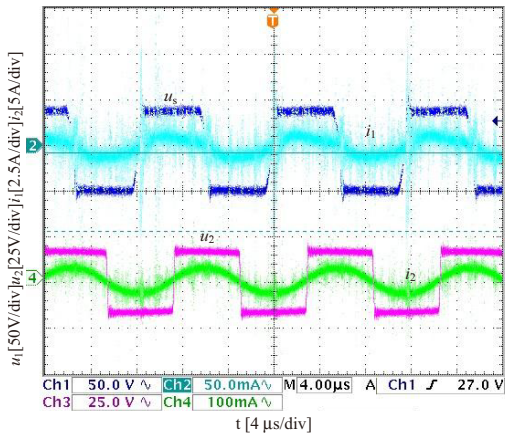

Figure 13. S-S compensation network experiment waveform.

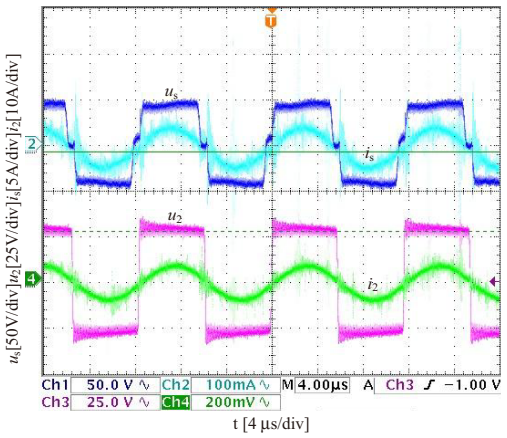

Figure 14. LCL-S compensation network experiment waveform.

From Fig. 15(a), it can be found that the charging current before and after optimization fluctuates around 0.5 A when R_b increases from 29.9 Ω to 47.2 Ω, which is mainly caused by the high-frequency equivalent resistance of coils and the loss of devise. The transmitting efficiency can realize over 80% using the proposed control strategy in CC mode, as shown in Fig. 16(a).

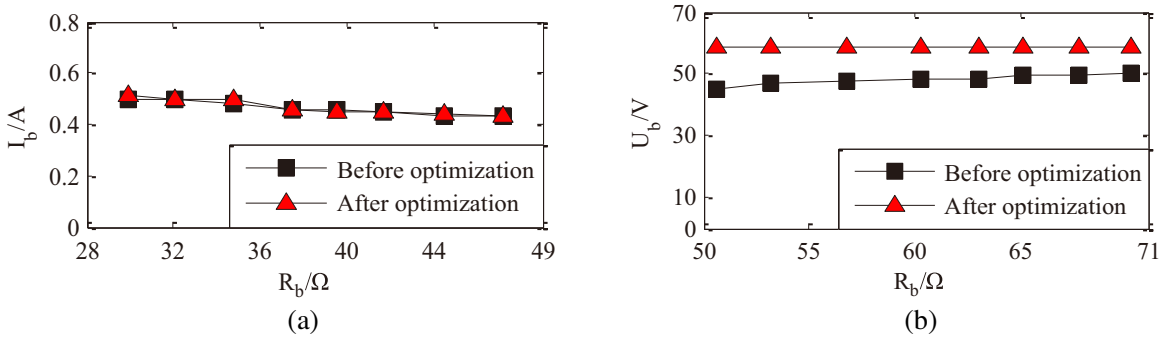

Figure 15. The CC/CV charging comparison experimental waveform before and after optimization. (a) The CC charging. (b) The CV charging.

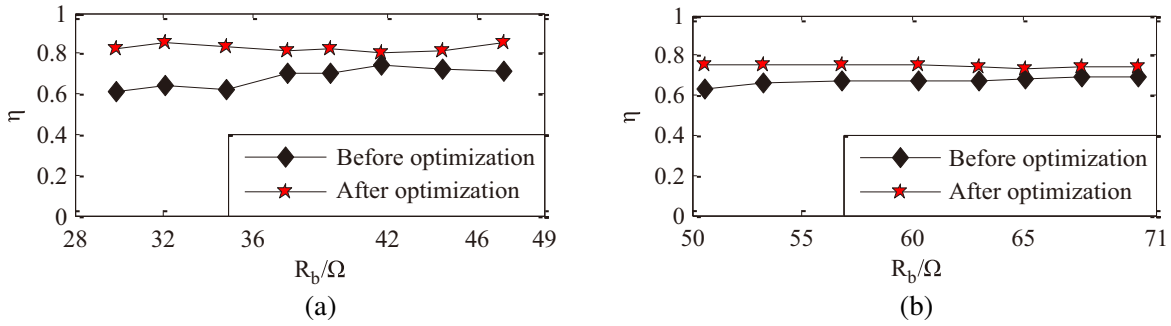

Figure 16. The transmission efficiency comparison experimental waveform before and after optimization in CC/CV mode. (a) CC mode. (b) CV mode.

Figure 15(b) depicts the trend of waveform before and after CV charging optimization. In CV mode, when R_b increases from 50.6 Ω to 70.2 Ω, the optimized charging voltage value has a certain deviation from the set voltage (50 V), but the stability of the charging voltage can be guaranteed. Fig. 16(b) shows that the transmitting efficiency can exceed 75% when the proposed control strategy is used.

It can be found that the variation of transmission efficiency before and after CC/CV charging optimization is respectively consistent with the simulation results shown in Fig. 11(a) and Fig. 11(b). Thus, the calculation results and simulation results above are certificated. Besides, as shown in Fig. 15(a), I_b is relatively constant when the load increases from 29.9 Ω to 47.2 Ω in CC charging mode. Similarly, as shown in Fig. 15(b), U_b is relatively constant when the load increases in a dynamic range in CV charging mode. It can be obviously found that CC/CV charging is maintained with arbitrary load impedance in the dynamic range. Moreover, the transmission efficiencies of CC/CV charging mode can maintain around 70% before optimization, as shown in Fig. 16(a) and Fig. 16(b). It can imply that CC/CV charging is maintained with the compensation network, and this compensation network is effective. Furthermore, the maximum transmission efficiencies in Fig. 16(a) and Fig. 16(b) are different, which may be caused by the unnecessary loss of the high-frequency equivalent resistances of compensation inductance L_{t1} and L_{t2} in LCL-S compensation network.

5. CONCLUSION

The article proposes a load-independence-based composite compensation network and the corresponding control strategy to achieve CC/CV charging of battery and transmitting efficiency optimization. The theoretical analysis of the network is given in this article. Then the control strategy is analyzed in detail, according to the characteristics of network. Finally, the results of the simulation and experiment show that the proposal not only realizes the CC/CV charging but also performs well in terms of the transmitting efficiency optimization.

In future work, the control strategy will be optimized to reduce the influence of coil parameter and circuit losses, and improve the transmission efficiency further.

ACKNOWLEDGMENT

This research was funded by the National Natural Science Foundation of China (Grant No. 51407084), the China Postdoctoral Science Foundation (Grant No. 2017M610294) and the Jiangsu Planned Projects for Postdoctoral Research Funds (Grant No. 1701092B).

REFERENCES

1. Budhia, M., J. T. Boys, G. A. Covic, and C. Huang, "Development of a single-sided flux magnetic coupler for electric vehicle IPT charging systems," *IEEE Transactions on Industrial Electronics*, Vol. 60, No. 1, 318–328, 2013.
2. Mohammad, M., S. Choi, Z. Islam, S. Kwak, and J. Baek, "Core design and optimization for better misalignment tolerance and higher range of wireless charging of PHEV," *IEEE Transactions on Transportation Electrification*, Vol. 3, No. 2, 445–453, 2017.
3. Kim, S., G. A. Covic, and J. T. Boys, "Tripolar pad for inductive power transfer systems for EV charging," *IEEE Transactions on Transportation Electrification*, Vol. 32, No. 7, 5045–5057, 2017.
4. Lee, I., N. Kim, and I. Cho, "Design of a patterned soft magnetic structure to reduce magnetic flux leakage of magnetic induction wireless power transfer systems," *IEEE Transactions on Electromagnetic Compatibility*, Vol. 59, No. 6, 1856–1863, 2017.
5. Kan, T., F. Lu, T. Nguyen, P. P. Mercier, and C. C. Mi, "Integrated coil design for EV wireless charging systems using LCC compensation topology," *IEEE Transactions on Power Electronics*, Vol. 33, No. 11, 9231–9241, 2018.
6. Kan, T., T. Nguyen, J. C. White, R. K. Malhan, and C. C. Mi, "A new integration method for an electric vehicle wireless charging system using lcc compensation topology: Analysis and design," *IEEE Transactions on Power Electronics*, Vol. 32, No. 2, 1638–1650, 2017.

7. Deng, J., W. Li, T. D. Nguyen, S. Li, and C. C. Mi, "Compact and efficient bipolar coupler for wireless power chargers: Design and analysis," *IEEE Transactions on Power Electronics*, Vol. 30, No. 11, 6130–6140, 2015.
8. Hu, J., F. Lu, and C. Zhu, "Hybrid energy storage system of an electric scooter based on wireless power transfer," *IEEE Transactions on Industrial Informatics*, Vol. 14, No. 9, 4169–4178, 2018.
9. Fu, M., H. Yin, X. Zhu, and C. Ma, "Analysis and tracking of optimal load in wireless power transfer systems," *IEEE Transactions on Power Electronics*, Vol. 30, No. 7, 3952–3963, 2015.
10. Mai, R., Y. Liu, Y. Li, P. Yue, G. Cao, and Z. He, "An active-rectifier-based maximum efficiency tracking method using an additional measurement coil for wireless power transfer," *IEEE Transactions on Power Electronics*, Vol. 33, No. 1, 716–728, 2018.
11. Berger, A., M. Agostinelli, S. Vesti, J. A. Oliver, J. A. Cobos, and M. Huemer, "A wireless charging system applying phase-shift and amplitude control to maximize efficiency and extractable power," *IEEE Transactions on Power Electronics*, Vol. 30, No. 11, 6338–6348, 2015.
12. Al-Haj Hussein, A. and I. Batarseh, "A review of charging algorithms for nickel and lithium battery chargers," *IEEE Transactions on Vehicular Technology*, Vol. 60, No. 3, 830–838, 2011.
13. Li, Y., Q. Xu, T. Lin, J. Hu, Z. He, and R. Mai, "Analysis and design of load-independent output current or output voltage of a three-coil wireless power transfer system," *IEEE Transactions on Transportation Electrification*, Vol. 4, No. 2, 364–375, 2018.
14. Tan, L., S. Pan, C. Xu, C. Yan, H. Liu, and X. Huang, "Study of constant current-constant voltage output wireless charging system based on compound topologies," *Journal of Power Electronics*, Vol. 17, No. 4, 1109–1116, 2017.
15. Cai, C., "Design and optimization of load-independent magnetic resonant wireless charging system for electric vehicles," *IEEE Access*, Vol. 6, 17264–17274, 2018.
16. Chen, Y., Z. Kou, Y. Zhang, Z. He, R. Mai, and G. Cao, "Hybrid topology with configurable charge current and charge voltage output-based WPT charger for massive electric bicycles," *IEEE Journal of Emerging and Selected Topics in Power Electronics*, Vol. 6, No. 3, 1581–1594, 2018.
17. Mai, R., Y. Chen, Y. Zhang, N. Yang, G. Cao, and Z. He, "Optimization of the passive components for an S-LCC topology-based WPT system for charging massive electric bicycles," *IEEE Transactions on Industrial Electronics*, Vol. 65, No. 7, 5497–5508, 2018.
18. Song, K., Z. Li, J. Jiang, and C. Zhu, "Constant current/voltage charging operation for series-series and series-parallel compensated wireless power transfer systems employing primary-side controller," *IEEE Transactions on Power Electronics*, Vol. 33, No. 9, 8065–8080, 2018.
19. Zhao, Q., A. Wang, J. Liu, and X. Wang, "The load estimation and power tracking integrated control strategy for dual-sides controlled LCC compensated wireless charging system," *IEEE Access*, Vol. 7, 75749–75761, 2019.
20. Zhang, M., L. Tan, J. Li, and X. Huang, "The charging control and efficiency optimization strategy for WPT system based on secondary side controllable rectifier," *IEEE Access*, Vol. 8, 127993–128004, 2020.
21. Huang, Z., C. Lam, and P. Mak, "A single-stage inductive-power-transfer converter for constant-power and maximum-efficiency battery charging," *IEEE Transactions on Power Electronics*, Vol. 35, No. 9, 8973–8984, 2020.
22. Huang, Z., S. Wong, and C. K. Tse, "Control design for optimizing efficiency in inductive power transfer systems," *IEEE Transactions on Power Electronics*, Vol. 33, No. 5, 4523–4534, 2018.
23. Li, Z., K. Song, and J. Jiang, "Constant current charging and maximum efficiency tracking control scheme for supercapacitor wireless charging," *IEEE Transactions on Power Electronics*, Vol. 33, No. 10, 9088–9100, 2018.